Application of the MoM-SO Method for Accurate Impedance Calculation of Single-Core Cables Enclosed by a Conducting Pipe

U. R. Patel, B. Gustavsen, and P. Triverio

***Abstract*—EMTP-type simulation programs include dedicated support routines for computing the series impedance of underground cables as a function of frequency. These routines take into account the skin effect in conductors but ignore any effect due to the proximity of the conductors. We introduce a new technique for calculating the series impedance which accurately predicts both skin and proximity effect. The method, which is based on an equivalent surface current representation, is highly efficient and is applicable to any arrangement of solid and hollow round conductors. We apply the proposed method, called MoM-SO, to a system of three single-core cables enclosed in a conductive pipe, achieving a speed up of more than 2000 times with respect to a finite elements solver. Time-domain simulation results demonstrate the influence of proximity effects on transient overvoltages.**

***Keywords*: Series impedance computation, wideband cable modeling, underground cables, electromagnetic transients.**

I. Introduction

The calculation of electromagnetic transients in power systems [1], [2], [3] requires the ability to model all network components with sufficient accuracy, taking into account their frequency-dependent behaviour. For underground cables, the modeling process starts with the computation of the per-unit-length (p.u.l) parameters of series impedance and shunt capacitance. The series impedance is always frequency-dependent due to skin effect in conductors and earth. Skin effect is easily accounted for by use of analytical formulae [4], [5]. In the case of three-phase cables, pipe type cables, and closely packed single-core cables, the series impedance is further affected by proximity effects which lead to an uneven (non-circular) current distribution on the conductors. This effect has traditionally been ignored since it can be predicted only with computationally expensive techniques, e.g. the Finite Element Method (FEM) [6].

Recently, the authors introduced MoM-SO [7], [8], a new method which is capable of accurately representing both skin and proximity effects for systems of solid, round conductors. This method, which is based on an equivalent surface current approach [9], is very fast and thus attractive for wide-band modeling of power cables.

In this paper, we extend the MoM-SO approach to include hollow conductors, a case not considered in previous works [9], [7], [8]. We outline the computational procedure but leave the detailed derivations for a future paper. Hollow conductors are particularly useful to represent metallic screens and pipes. Then, we apply MoM-SO to the modeling of three single-core cables that include a tubular screen and are enclosed by a conducting pipe. The series impedance of this seven-conductor system is calculated over a wide frequency band and the result is validated against a FEM computation. The impedance is next used as input for the Universal Line Model (ULM) [10] in order to simulate transient overvoltages on the phase conductors and the metallic sheaths. The significance of taking the proximity effect into account is highlighted.

II. Series Impedance Computation Through a Surface Admittance Operator

A. Problem description

In this work, we consider the modeling of cables made by several conductors of circular shape, such as the configuration shown in Fig. 1. We allow for both solid and hollow conductors. Solid conductors are used for modeling the phase conductors but can also be used for representing the individual strands of a wire screen or of a stranded armoring as in [7]. Hollow conductors can represent tubular sheath conductors (metallic screens), enclosing pipes, and hollow phase conductors of oil-filled cables that include an oil channel. Hollow conductors can also be used for approximately representing wire screens and stranded armors, with great savings in computation time.

We let P be the total number of conductors present in the cable, either solid or hollow, and we denote the potential of the p-th conductor as V_p. To simplify the notation, all potentials are collected in a column vector

$$\mathbf{V} = \begin{bmatrix} V_1 & V_2 & \dots & V_P \end{bmatrix}^T . \tag{1}$$

This work was supported in part by the KPN project "Electromagnetic transients in future power systems" (ref. 207160/E20) financed by the Norwegian Research Council (RENERGI programme) and by a consortium of industry partners led by SINTEF Energy Research: DONG Energy, EdF, EirGrid, Hafslund Nett, National Grid, Nexans Norway, RTE, Siemens Wind Power, Statnett, Statkraft, and Vestas Wind Systems.

U. R. Patel and P. Triverio are with the Edward S. Rogers Sr. Department of Electrical and Computer Engineering, University of Toronto, Toronto, M5S 3G4 Canada (email: utkarsh.patel@mail.utoronto.ca, piero.triverio@utoronto.ca).

B. Gustavsen is with SINTEF Energy Research, Trondheim N-7465, Norway (e-mail: bjorn.gustavsen@sintef.no).

Paper submitted to the International Conference on Power Systems Transients (IPST2013) in Vancouver, Canada July 18-20, 2013.

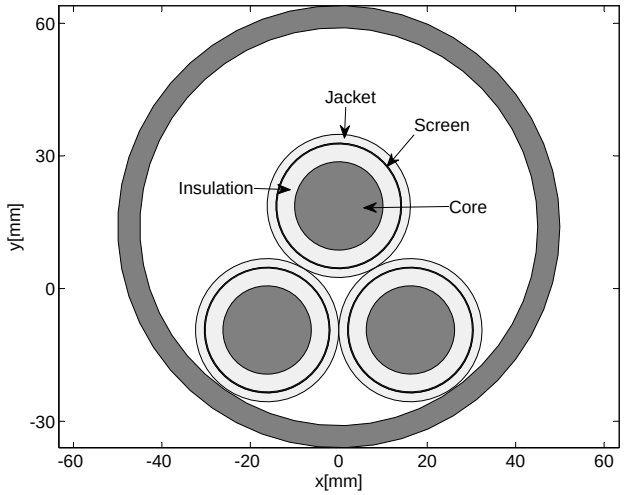

Fig. 1. Three single-core cables inside a conducting pipe (seven conductors).

Similarly, we define the vector of conductor currents

$$\mathbf{I} = \begin{bmatrix} I_1 & I_2 & \dots & I_P \end{bmatrix}^T , \tag{2}$$

where I_p is the current flowing in the p-th conductor. The transmission line equation [11]

$$\frac{\partial \mathbf{V}}{\partial z} = -\left[\boldsymbol{\mathscr{R}}(\omega) + j\omega\boldsymbol{\mathscr{L}}(\omega)\right]\mathbf{I} \tag{3}$$

relates $\mathbf{V}$ and $\mathbf{I}$ through the p.u.l. resistance matrix $\boldsymbol{\mathscr{R}}(\omega)$ and the p.u.l. inductance matrix $\boldsymbol{\mathscr{L}}(\omega)$ of the cable. Our objective is to compute $\boldsymbol{\mathscr{R}}(\omega)$ and $\boldsymbol{\mathscr{L}}(\omega)$ for a given set of frequency values. Once these matrices are available, one can compute several quantities of interest for cable analysis, such as positive- and zero-sequence impedance at the operating and harmonic frequencies. Also, the computed samples can be used as input parameters for the broadband cable models used in EMTP transient analysis. In Sec. III we will demonstrate such usage based on the geometry in Fig. 1.

B. Surface Admittance Operator for Solid Conductors

In order to compute the series impedance of the cable, we follow the surface approach of [9], which takes as unknown the electric field on the surface of each conductor. The field distribution inside the conductors is modelled implicitly with a surface admittance operator. We first present this concept for a solid conductor like the one shown in the left panel of Fig. 2.

We denote the longitudinal electric field on the conductor surface by $E_z^{(p)}(\theta)$, where θ is the angular coordinate shown in Fig. 2. Motivated by the circular symmetry of the conductor, we approximate the field distribution with a truncated Fourier series

$$E_z^{(p)}(\theta) \;=\; \sum_{n=-N_p}^{N_p} E_n^{(p)} e^{jn\theta} , \tag{4}$$

where the truncation order N_p controls the fidelity of the approximation. Using the equivalence theorem [12], we replace

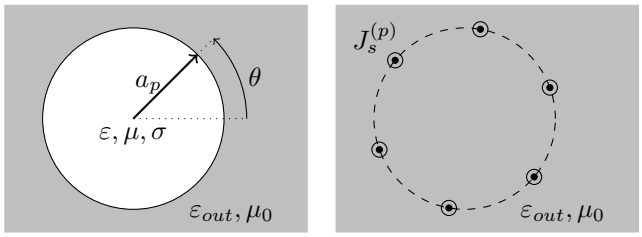

Fig. 2. Application of the equivalence theorem to a solid round conductor. The conductor (left panel) is replaced by the surrounding medium and an equivalent current $J_s^{(p)}$ on its surface (right panel). The conductor radius is denoted with a_p.

the conductor with the surrounding medium, and we introduce an equivalent current $J_s^{(p)}(\theta)$ on the conductor surface. This transformation is depicted in Fig. 2. We let the equivalent current be expressed in a Fourier series analogous to (4)

$$J_s^{(p)}(\theta) \;=\; \frac{1}{2\pi a_p} \sum_{n=-N_p}^{N_p} J_n^{(p)} e^{jn\theta} , \tag{5}$$

where a_p is the radius of the conductor. If a suitable relation between the electric field (4) and the equivalent current (5) is enforced, the transformation does not alter the electric field *outside* the conductor. Such relation is given by a surface admittance operator [9]. In terms of the coefficients of (4) and (5), the operator for a round conductor reads

$$J_n^{(p)} = Y_n^{(p)} E_n^{(p)} , \tag{6}$$

where the surface admittance coefficients $Y_n^{(p)}$ are given by [9]

$$Y_n^{(p)} = \frac{2\pi}{j\omega}\left[\frac{ka_p\mathcal{J}'_{|n|}(ka_p)}{\mu\mathcal{J}_{|n|}(ka_p)} - \frac{k_{out}a_p\mathcal{J}'_{|n|}(k_{out}a_p)}{\mu_0\mathcal{J}_{|n|}(k_{out}a_p)}\right] . \tag{7}$$

In (7), $\mathcal{J}_{|n|}(.)$ is the Bessel function of the first kind [13] of order $|n|$, and $\mathcal{J}'_{|n|}(.)$ is its derivative. The quantity $k = \sqrt{\omega\mu(\omega\varepsilon - j\sigma)}$ is the wavenumber in the conductor material, which has permittivity ϵ, conductivity σ, and permeability μ. Similarly, $k_{out} = \omega\sqrt{\mu_0\varepsilon_{out}}$ is the wavenumber in the surrounding medium, which has permittivity ε_{out}, permeability μ_0, and is assumed to be lossless. After applying the surface admittance operator to each conductor, we obtain an equivalent configuration where the medium is homogeneous, greatly facilitating the computation of the series impedance. Before discussing this step in Sec. II-D, we extend the surface admittance approach to hollow round conductors, such as the one shown in the left panel of Fig. 3.

C. Surface Admittance Operator for Hollow Conductors

The main difference from the solid case is the presence of two boundaries between the conductor and the surrounding medium. We approximate the field on the outer boundary with (4) and, for the field on the inner boundary, we introduce the Fourier series

$$E_z^{(p,i)}(\theta) \;=\; \sum_{n=-N_p}^{N_p} E_n^{(p,i)} e^{jn\theta} . \tag{8}$$

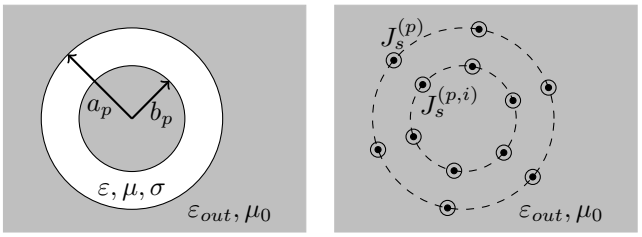

Fig. 3. Application of the equivalence theorem to a hollow conductor. The actual conductor, shown in the left panel, is replaced by the surrounding medium and equivalent currents $J_s^{(p,i)}$ and $J_s^{(p)}$ are introduced on the inner and outer surface of the conductor (right panel). The inner and outer radius are denoted with b_p and a_p, respectively.

With the equivalence theorem, we replace the conductor with the surrounding medium, as shown in Fig. 3. Two equivalent current densities are introduced, one on the outer boundary given by (5), and one on the inner boundary given by

$$J_s^{(p,i)}(\theta) \quad = \quad \frac{1}{2\pi b_p} \sum_{n=-N_p}^{N_p} J_n^{(p,i)} e^{jn\theta}\,, \tag{9}$$

where b_p is the inner radius of the conductor. The value of the equivalent currents is chosen in such a way that the transformation will not alter the electric and magnetic field both inside the cavity and outside the conductor. Generalizing the approach of [9], we proved that the equivalent currents are related to field coefficients by a 2×2 surface admittance matrix

$$\begin{bmatrix} J_n^{(p,i)} \\ J_n^{(p)} \end{bmatrix} = \begin{bmatrix} Y_{11,n}^{(p)} & Y_{12,n}^{(p)} \\ Y_{21,n}^{(p)} & Y_{22,n}^{(p)} \end{bmatrix} \begin{bmatrix} E_n^{(p,i)} \\ E_n^{(p)} \end{bmatrix} \tag{10}$$

which is a generalization of (7). The entries of the matrix are given by

$$\begin{aligned}
Y_{11,n}^{(p)} &= \frac{2\pi}{j\omega}\left[\frac{\chi_n(ka_p, kb_p)}{m_n(ka_p, kb_p)\mu} - \frac{\chi_n(k_{out}a_p, k_{out}b_p)}{m_n(k_{out}a_p, k_{out}b_p)\mu_0}\right] \\
Y_{12,n}^{(p)} &= \frac{2\pi}{j\omega}\left[\frac{\chi_n(k_{out}b_p, k_{out}b_p)}{m_n(k_{out}a_p, k_{out}b_p)\mu_0} - \frac{\chi_n(kb_p, kb_p)}{m_n(ka_p, kb_p)\mu}\right] \\
Y_{21,n}^{(p)} &= \frac{2\pi}{j\omega}\left[\frac{\chi_n(k_{out}a_p, k_{out}a_p)}{m_n(k_{out}a_p, k_{out}b_p)\mu_0} - \frac{\chi_n(ka_p, ka_p)}{m_n(ka_p, kb_p)\mu}\right] \\
Y_{22,n}^{(p)} &= \frac{2\pi}{j\omega}\left[\frac{\chi_n(kb_p, ka_p)}{m_n(ka_p, kb_p)\mu} - \frac{\chi_n(k_{out}b_p, k_{out}a_p)}{m_n(k_{out}a_p, k_{out}b_p)\mu_0}\right]
\end{aligned}$$

where

$$\chi_n(\alpha, \beta) = \beta\left[\mathcal{H}'_{|n|}(\beta)\mathcal{K}_{|n|}(\alpha) - \mathcal{H}_{|n|}(\alpha)\mathcal{K}'_{|n|}(\beta)\right] \tag{11}$$

$$m_n(\alpha, \beta) = \mathcal{H}_{|n|}(\alpha)\mathcal{K}_{|n|}(\beta) - \mathcal{H}_{|n|}(\beta)\mathcal{K}_{|n|}(\alpha)\,. \tag{12}$$

In (11) and (12), $\mathcal{H}_{|n|}(.)$ and $\mathcal{K}_{|n|}(.)$ are the Hankel functions of order $|n|$ of the first and second kind [13], respectively. The functions $\mathcal{H}'_{|n|}(.)$ and $\mathcal{K}'_{|n|}(.)$ are the corresponding derivatives. Because of the limited space, we omit the proof of these relations, which will be given in a future publication. The surface admittance relations (7) and (10), written for all conductors of the cable, can be summarized by the matrix relation

$$\mathbf{J} = \mathbf{Y}_s \mathbf{E}\,, \tag{13}$$

where the column vector $\mathbf{E}$ collects all field coefficients $E_n^{(p)}$ and $E_n^{(p,i)}$. Similarly, the vector $\mathbf{J}$ collects all coefficients of (5) and (9).

D. Electric Field Integral Equation

After replacing each conductor with the surrounding medium, we obtain a simpler electromagnetic problem with a uniform medium. Using the electric field integral equation [14], we can write the electric field at a point $\vec{r}$ as

$$E_z(\vec{r}) = j\omega\mu_0 \int J_s(\vec{r}\,')G\left(\vec{r}, \vec{r}\,'\right) d\vec{r}\,' - \frac{\partial V}{\partial z}\,. \tag{14}$$

where

$$G(\vec{r}, \vec{r}\,') = \frac{1}{2\pi} \ln|\vec{r} - \vec{r}\,'| \tag{15}$$

is the Green's function of a homogeneous bi-dimensional space [9]. The first term in (14) is the field produced by the equivalent currents that replaced the conductors. Integration is performed over the outer boundary of each conductor and, for hollow conductors, also over the inner boundary. The second term is related to the electrostatic potential V. In order to solve integral equation (14) numerically, we discretize it into a set of algebraic equations with the method of moments [15], a popular technique to solve numerically integral and differential equations. This process, described in [7], eventually leads to the following numerical counterpart of (14)

$$\mathbf{E} = j\omega\mu_0 \mathbf{G}\mathbf{J} - \mathbf{U}\frac{\partial \mathbf{V}}{\partial z}\,, \tag{16}$$

where the matrix $\mathbf{G}$ is the discrete version of the Green's function (15). The entries of $\mathbf{G}$ can be computed analytically by solving a double integral [7]. The constant matrix $\mathbf{U}$ follows from the relation

$$\mathbf{I} = \mathbf{U}^T \mathbf{J}\,. \tag{17}$$

between the line currents $\mathbf{I}$ and the equivalent current coefficients $\mathbf{J}$. Substituting (3) into (16), we obtain

$$\mathbf{E} = j\omega\mu_0 \mathbf{G}\mathbf{J} + \mathbf{U}\left[\boldsymbol{\mathscr{R}}(\omega) + j\omega\boldsymbol{\mathscr{L}}(\omega)\right]\mathbf{I}\,. \tag{18}$$

E. Computation of the Series Impedance

By combining (13) and (18) we obtain, with a few algebraic manipulations [7], the final formula for computing the series resistance and inductance of the cable

$$\boldsymbol{\mathscr{R}}(\omega) + j\omega\boldsymbol{\mathscr{L}}(\omega) = \left[\mathbf{U}^T(\mathbf{1} - j\omega\mu_0 \mathbf{Y}_s \mathbf{G})^{-1}\mathbf{Y}_s\mathbf{U}\right]^{-1}\,. \tag{19}$$

III. Example: Three Single-Core Cables Enclosed Within a Conducting Pipe

A. Cable Description

To demonstrate the versatility and accuracy of the MoM-SO approach, we apply it to a configuration of three single-core coaxial cables that are placed asymmetrically inside a conducting pipe (see Fig. 1). Each single-core cable features a metallic screen inside an insulating jacket, giving a system of seven insulated conductors. We remark that three-phase cables and pipe-type cables can be viewed as subclasses of

TABLE I
CHARACTERISTICS OF THE CABLE SYSTEM SHOWN IN FIG. 1.

Item	Parameters
Core	$\sigma = 58 \cdot 10^6$ S/m, radius = 10.0 mm
Insulation	Thickness = 4.0 mm, $\epsilon_r = 2.3$
Screen	Thickness = 0.2 mm, $\sigma = 58 \cdot 10^6$ S/m
Jacket	Thickness = 2 mm, $\epsilon_r = 2.3$
Steel pipe	Outer diameter = 100 mm, thickness = 5 mm, $\sigma = 10^7$ S/m , $\mu_r = 100$

the geometry in Fig. 1. The three-phase cable has its single-core cables symmetrically placed inside the equivalent pipe conductor (armoring), while the pipe-type cable has its single-core cables asymmetrically arranged inside the pipe but with metallic screens touching. Most EMTP-type programs include a procedure for computing the cable series impedance which in the case of symmetrically arranged single-core cables partially accounts for proximity effects in the pipe [5], but not in the phase conductors and screens.

B. Series Impedance Computation

Using MoM-SO, we computed the 6×6 series impedance matrix with respect to the six conductors (three phase conductors plus three screens), between 1 Hz and 1 MHz using 120 logarithmically spaced samples. Next, the screens were eliminated by assuming them to be continuously grounded, giving a 3×3 impedance matrix. Figure 4 shows the calculated positive sequence resistance and inductance per km, for different truncation orders of the Fourier series (4), (5), (8) and (9). It is observed that orders $N_p = 3$ and $N_p = 7$ practically give the same result, and so $N_p = 3$ is deemed sufficient. For validation, we compared MoM-SO against a FEM simulation [6] performed with a fine mesh (108,418 triangles). The MoM-SO result agrees very closely with the FEM result, thereby validating the proposed algorithm. Figure 4 also shows the cable parameters obtained with $N_p = 0$. With this setting, we assume a circularly-symmetric current distribution in the conductors, neglecting proximity effects. The results in Fig. 4 show that this common assumption leads to a noticeable deviation for the resistance and in particular for the inductance.

Fig. 5 shows the same result when the screens have not been eliminated, i.e. with zero net current flowing in each screen. It is observed that we now get large errors also at high frequencies when ignoring the proximity effect ($N_p = 0$), while the result with MoM-SO ($N_p = 3$, $N_p = 7$) agrees closely with the FEM solution. In this case, the screens can only partially shield the magnetic field as only proximity currents are permitted to circulate in the screens. As before, $N_p = 3$ is a sufficient order for MoM-SO since increasing the order to $N_p = 7$ does not change the result.

C. Timing Results

Table II reports the computational efficiency for the alternative approaches. FEM takes 3.5 hours to compute the cable impedance, while MoM-SO with $N_p = 3$ takes only 5.57 s. The proposed method is therefore faster by a factor of about 2200. These results confirm the outstanding efficiency of the proposed method.

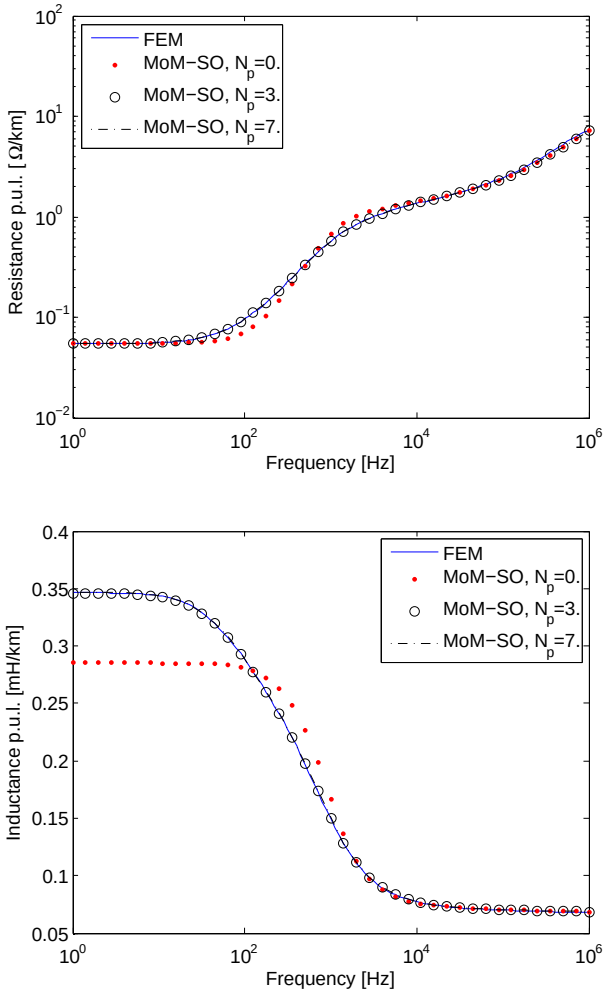

Fig. 4. P.u.l. positive sequence resistance and inductance of the cable system, obtained with MoM-SO and FEM. Screens are continuously grounded.

TABLE II
COMPUTATION TIME FOR THE PROPOSED METHOD (MOM-SO) AND FINITE ELEMENTS (FEM) APPLIED TO THE CABLE SYSTEM OF SEC. III. ALL COMPUTATIONS WERE PERFORMED ON A WORKSTATION WITH A 2.5 GHZ CPU AND 16 GB OF MEMORY.

Method	Computation time	Speed up
FEM	12,600 s = 3.5 hours	-
MoM-SO, $N_p = 0$	3.57 s	3529 X
MoM-SO, $N_p = 3$	5.57 s	2262 X
MoM-SO, $N_p = 7$	7.93 s	1589 X

D. Traveling Wave Modeling by Universal Line Model

The shunt capacitance matrix $\mathscr{C}$ was calculated under the assumption that the cable is filled with a poorly conductive medium, allowing standard analytical formulae to be used [4]. The capacitance value, and the resistance and inductance values obtained from MoM-SO with $N_p = 3$, were used to compute the characteristic admittance matrix $\mathbf{Y}_c$ and the propagation function $\mathbf{H}$ of the cable, assuming a length of $l = 1$ km. The samples were next subjected to rational modeling by the Universal Line Model [10]. Figs. 6 and 7 compare the raw samples of $\mathbf{Y}_c$ and $\mathbf{H}$ with the extracted model, showing an excellent agreement between the two.

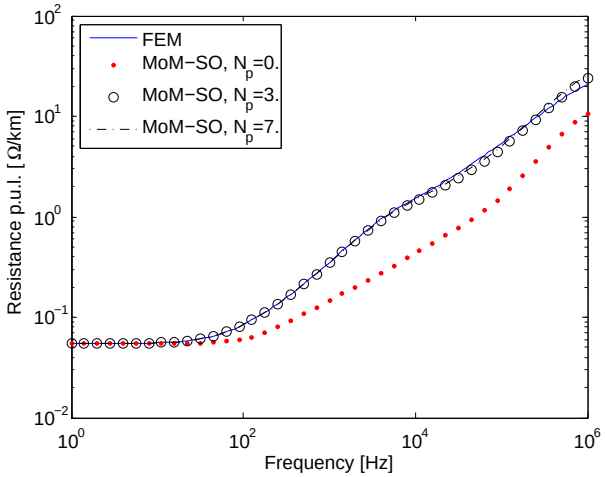

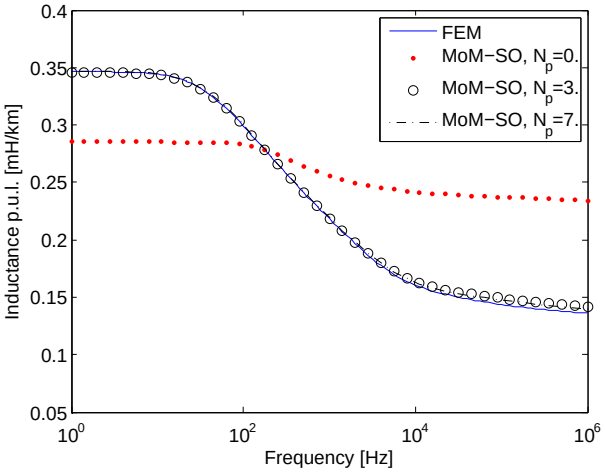

Fig. 5. P.u.l. positive sequence resistance and inductance of the cable system, obtained with MoM-SO and FEM. Screens are open.

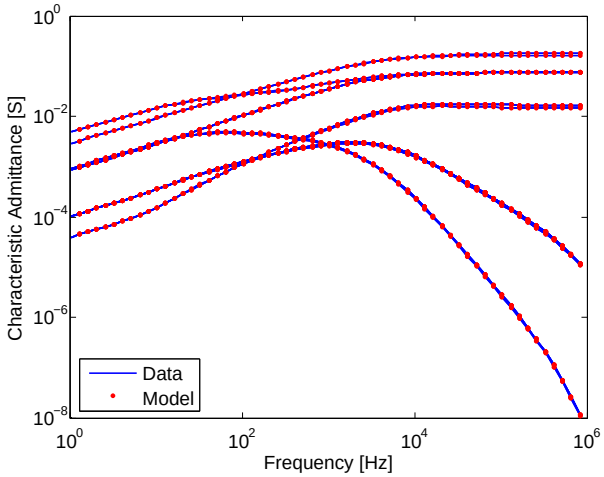

Fig. 6. Rational fitting of the characteristic admittance $\mathbf{Y_c}$ of the cable system of Sec. III. The initial samples (solid blue curve) are compared with the response of the extracted model (red dots). An approximation of order 14 has been used.

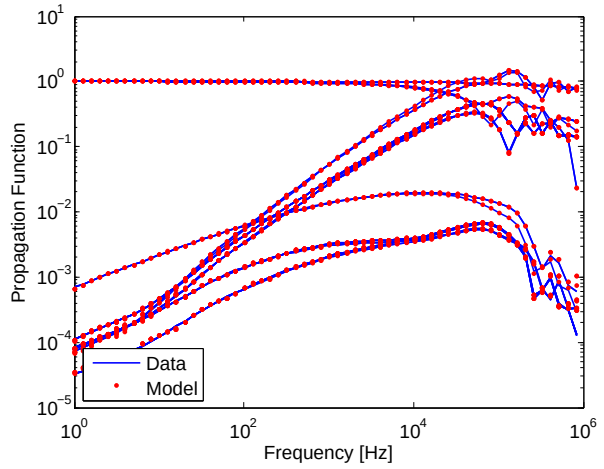

Fig. 7. Rational fitting of the propagation function $\mathbf{H}$ of the cable system of Sec. III. The initial samples (solid blue curve) are compared with the response of the extracted model (red dots). The extracted model has order 10 for each of the four group delays [10].

E. Transient Waveforms

Using the time domain implementation of the Universal Line Model available in PSCAD v4.2 [16], a transient voltage response was calculated when applying a unit step voltage to the phase conductor of the top cable in Fig. 1, with all other phases and sheaths grounding at one end. All conductors are open at the far end, as shown in Fig. 8. Figures 9 and 10 show respectively the resulting voltage waveforms between the phase and screen, and between the phase and ground. Simulations were performed three times using the series impedance obtained with different methods: FEM, MoM-SO with $N_p = 0$ (only skin effect taken into account), and MoM-SO with $N_p = 3$ (both skin and proximity effect taken into account). It is observed that the induced sheath voltage is strongly affected by the proximity effect and that the result by MoM-SO ($N_p = 3$) and FEM agree closely. The deviation from the FEM result is further reduced when increasing the MoM-SO order.

The effect of proximity is even more pronounced for waves that travel between the sheaths, i.e. the intersheath modes. To see this, we applied a step voltage between the sheaths of the two lower cables in Fig. 1 as shown in Fig. 11. The simulated results in Fig. 12 show that ignoring proximity effect leads to very large errors in the transient response.

IV. Conclusion

We presented a fast and accurate technique to compute the series impedance of cables with round conductors. The method supports both solid and hollow (tubular) conductors, and accurately predicts both skin and proximity effect. Compared to existing approaches, like finite elements, the proposed method is much faster, and we demonstrated a speed up of 2200X in the modeling of three single-core cables enclosed by a conducting pipe. The simulated transient overvoltages also show the importance of an accurate prediction of proximity effects.

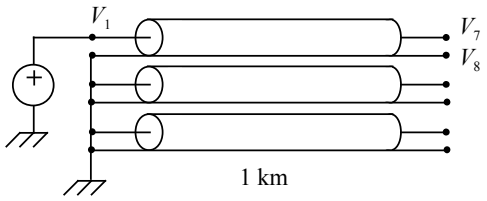

Fig. 8. First configuration considered in Sec. III-E. A unit step voltage is applied to the top phase conductor of the cable of Fig. 1. All other phases and sheaths are grounded at one end.

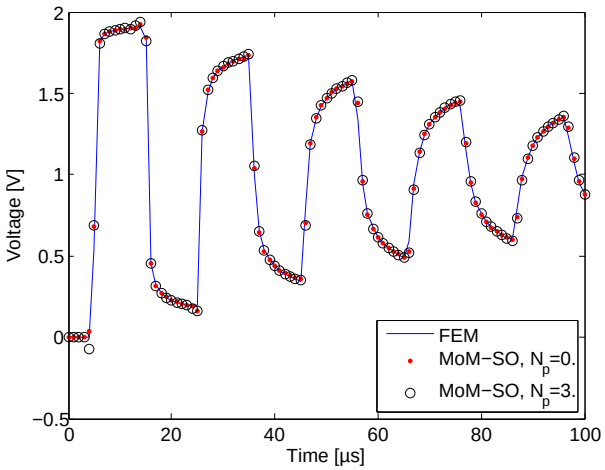

Fig. 9. Phase-screen voltage at the receiving end ($V_7 - V_8$) for the configuration show in Fig. 8.

REFERENCES

[1] P. Chowdhuri, *Electromagnetic transients in power systems*. Research Studies Press, 1996.

[2] H. W. Dommel, "Digital computer solution of electromagnetic transients in single-and multiphase networks," *IEEE Trans. on Power Apparatus and Systems*, no. 4, pp. 388–399, 1969.

[3] J. Mahseredjian, S. Dennetire, L. Dub, B. Khodabakhchian, and L. Grin-Lajoie, "On a new approach for the simulation of transients in power systems," *Electric Power Systems Research*, vol. 77, no. 11, pp. 1514 – 1520, 2007.

[4] L. Wedepohl and D. Wilcox, "Transient analysis of underground power-transmission systems. System-model and wave-propagation characteristics," *Proceedings of the IEEE*, vol. 120, no. 2, pp. 253 –260, Feb. 1973.

[5] A. Ametani, "A general formulation of impedance and admittance of cables," *IEEE Trans. Power Apparatus and Systems*, no. 3, pp. 902–910, 1980.

[6] B. Gustavsen, A. Bruaset, J. Bremnes, and A. Hassel, "A finite element approach for calculating electrical parameters of umbilical cables," *IEEE Trans. Power Delivery, vol. 24, no. 4, pp. 2375-2384*, Oct. 2009.

[7] U. R. Patel, B. Gustavsen, and P. Triverio, "Fast Computation of the Series Impedance of Power Cables with Inclusion of Skin and Proximity Effects," *IEEE Trans. on Power Delivery*, Submitted.

[8] ——, "MoM-SO: a Fast and Fully-Automated Method for Resistance and Inductance Computation in High-Speed Cables," *17th IEEE Workshop on Signal and Power Integrity*, Paris, France, May 12-15, 2013. Submitted.

[9] D. De Zutter, and L. Knockaert, "Skin Effect Modeling Based on a Differential Surface Admittance Operator," *IEEE Trans. on Microwave Th. and Tech.*, Aug. 2005.

[10] A. Morched, B. Gustavsen, M. Tartibi, "A universal model for accurate calculation of electromagnetic transients on overhead lines and underground cables," *IEEE Trans. Power Delivery*, vol. 14, no. 3, pp. 1032–1038, 1999.

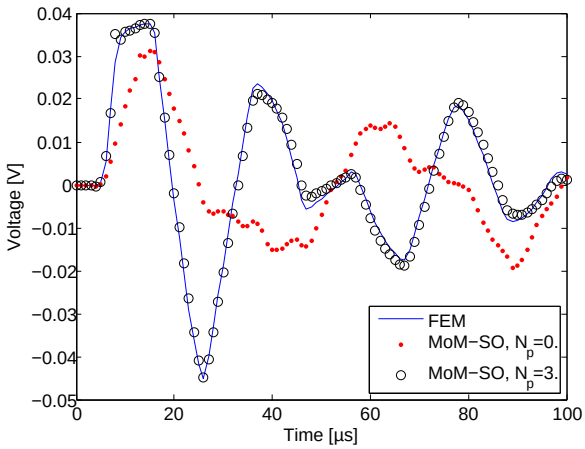

Fig. 10. Sheath voltage at the receiving end (V_8) for the configuration show in Fig. 8.

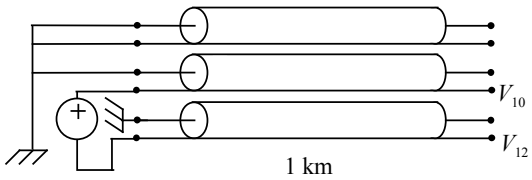

Fig. 11. Second configuration considered in Sec. III-E. A differential voltage excitation is applied between two screens.

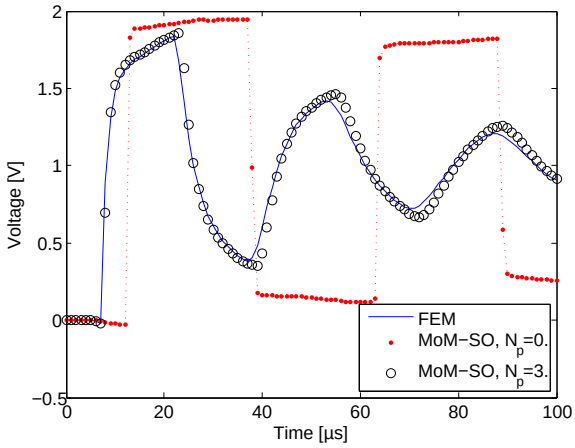

Fig. 12. Differential voltage at the receiving end ($V_{10} - V_{12}$) for the configuration of Fig. 11.

[11] C. R. Paul, *Analysis of Multiconductor Transmission Lines*, 2nd ed. Wiley, 2007.

[12] R. F. Harrington, *Time-Harmonic Electromagnetic Fields*. McGraw-Hill, 1961.

[13] M. Abramowitz and I. A. Stegun, *Handbook of Mathematical Functions with Formulas, Graphs, and Mathematical Tables*. New York: Dover, 1964.

[14] C. A. Balanis, *Antenna Theory: Analysis and Design*, 3rd ed. Wiley, 2005.

[15] W. C. Gibson, *The Method of Moments in Electromagnetics*. Chapman & Hall/CRC, 2008.

[16] Pscad homepage. Manitoba Hydro International Limited. [Online]. Available: https://hvdc.ca/pscad/